Int. J. Heat Mass Transfer. Vol. 36, No. 2, pp. 453–462, 1993
Printed in Great Britain

0017–9310/93 $6.00 + 0.00
© 1993 Pergamon Press Ltd

# A photographic method for the visualization of mass uptake patterns in aqueous systems

A. DASGUPTA, P. GUENARD and J. S. ULTMAN†
Department of Chemical Engineering, Pennsylvania State University, University Park, PA 16802, U.S.A.

and

J. S. KIMBELL and K. T. MORGAN
Chemical Industry Institute of Toxicology, Research Triangle Park, NC 27709, U.S.A.

(*Received* 28 *August* 1991 *and in final form* 24 *January* 1992)

**Abstract**—A new method utilizing the flow of dilute developer solution over an exposed photographic film was employed for visualizing mass uptake patterns at a solid surface. For flow around a backward-facing step, the developed film revealed mass transfer from a corner eddy, circulating stall and reattachment point. Along the floor of a rectangular channel containing a vertical cylinder or a vertical square plate, the developed film displayed a horseshoe-shaped high mass transfer region upstream of the obstruction and a wake-like high mass transfer region downstream of the obstruction.

## INTRODUCTION

ALTHOUGH new and improved techniques of flow visualization such as hot-film anemometry and laser–Doppler velocimetry are frequently reported, the determination of mass uptake patterns at solid boundaries has received little recent attention. Yet, many problems in science and engineering are related to the effect of fluid mechanics on the diffusion of materials to reactive and/or permeable surfaces. Flush-mounted redox electrodes are one means of measuring local mass transfer coefficients [1]. Although arrays of such electrodes could, in principle, be used to determine a detailed distribution of mass uptake, difficulties in fabrication and performance limit their usefulness.

In contrast, profilometric techniques are quite simple to implement: test fluid is directed over a surface which has been coated with a material that recedes in proportion to the local mass transfer rate. The most common coatings have been pure solids which either sublime into a flowing test gas or dissolve into a test liquid [2, 3]. Alternatively, the surface can be coated with a polymer which is initially loaded with a swelling agent [4, 5]. As the swelling agent is eluded from the polymer by the test fluid, the polymer shrinks. Such a polymer, which is permanently attached to the surface, has two advantages over a subliming or dissolving solid coating. First, a polymer-coated surface can be used repeatedly, as long as it can be recharged with swelling agent. Second, it is possible to employ the same polymer coating for both gas and liquid phase diffusion studies by the appropriate selection of volatile and soluble swelling agents.

The main difficulty in profilometric methods is determining the local recession of the surface coating. A breakthrough in this problem has been the application of holographic interferometry techniques which work well for both transparent and opaque polymer coatings [6, 7]. However, holographic interferometry requires a technically-demanding and expensive optical apparatus which must be integrated into the experimental system. It is the purpose of the present technical note to describe a new and much simpler method for visualizing mass uptake patterns.

This method is based on the chemical development of a photographic emulsion, a process whose rate depends on convective-diffusion in the developer solution. In particular, a totally-exposed photographic film is attached to a surface, and developer is circulated over the surface for a known interval of time. The resulting image on the fixed emulsion serves as a permanent qualitative record of the spatial distribution of mass uptake. The image may be quantified in terms of optical density (OD) by using a scanning densitometer designed for reading gel chromatographs.

## METHODS AND MATERIALS

A photographic film consists of an emulsion-coated transparent support, normally a derivative of cellu-

† Author to whom all correspondence should be addressed.

lose. The emulsion contains a large number of minute crystals of silver halide suspended in gelatin. During the process of film development, the transparent silver halide crystals which were previously exposed to light are reduced to opaque filamentous silver, and this results in a local increase in OD of the emulsion. In the aqueous developer used in this study (Kodak D-76 Developer), hydroquinone diffuses to the emulsion surface where its anion can donate two electrons for the reduction of silver halide to metallic silver and halide anion. Although controversy surrounds the question of whether it is the hydroquinone anions or the electrons that diffuse into the gelatin layer, it is clear that the reduction reaction is sufficiently fast that the convective-diffusion of hydroquinone to the emulsion surface strongly influences development rate [8]. Therefore, the rate of increase in OD of the emulsion is a qualitative indication of the diffusion resistance of hydroquinone through the aqueous phase.

In the experiments we conducted, a 100 ASA black and white sheet film (Kodak Plus-X) was pre-exposed for 20 min to a 100 W incandescent bulb positioned 15 cm from the emulsion. After securing the film to the wall of a test section, developer solution was circulated over the emulsion for a known period of time. Next, the film was immersed in a stop bath (Kodak Stop Bath) for 30 s, fixed for 5 min (Kodak Fixer), and thoroughly rinsed in order to preserve the optical density changes created by the diffusion of hydroquinone to the emulsion surface. In the resulting photographic negatives, high mass transfer rates appeared as opaque (i.e. high OD) regions while low mass transfer rates appeared as transparent (i.e. low OD) regions. The values of OD presented in Figs. 2, 3, 8, 11 and 14 of this report were obtained by reading the negatives with a gel chromatogram scanner (Model 620, Bio-rad). Also included as Figs. 4, 7, 9, 10, 12 and 13 are positive prints of the negatives in which high mass transfer rates appear as white and low mass transfer rates appear as black.

The potential resolution of the photographic method was evaluated by comparing OD obtained in quiescent and in well-mixed developer solutions. In one series of experiments, 3.5 × 1 cm strips of exposed film were taped to the sides of a beaker containing one liter of unstirred developer solution. Different film strips were developed for alternative times from 1 to 200 min in solutions that had been diluted by 5-, 10-, and 40-fold from a standard stock solution. The stock solution was prepared from the dry D-76 formulation according to manufacturer's instructions. In a second series of experiments, a high-speed agitator was suspended in the beaker and the same development times and D-76 dilutions were studied under well-mixed conditions. Following these experiments, OD scans along three different paths of each film strip were averaged to obtain a mean OD value.

The ability of the photographic method to record mass uptake patterns was tested in a 91.4 cm long and 20.3 cm wide open channel containing a 12.7 cm depth of flowing developer solution (Fig. 1). Liquid entered this rectangular test section through a stack of soda straws acting as flow straighteners, and liquid exiting the test section was recirculated through a rectangular recycle duct by a 4 in. shrouded propeller. Dye streakline analysis was used to characterize the flow fields produced at a low, an intermediate and a high speed setting of the propeller motor: pulses of a 1% aqueous solution of basic fuchsin were manually injected through a movable capillary inlet tube located at a series of vertical positions in the midplane of the test section, and local velocity was determined by frame-by-frame analysis of a video recording of the dye movement.

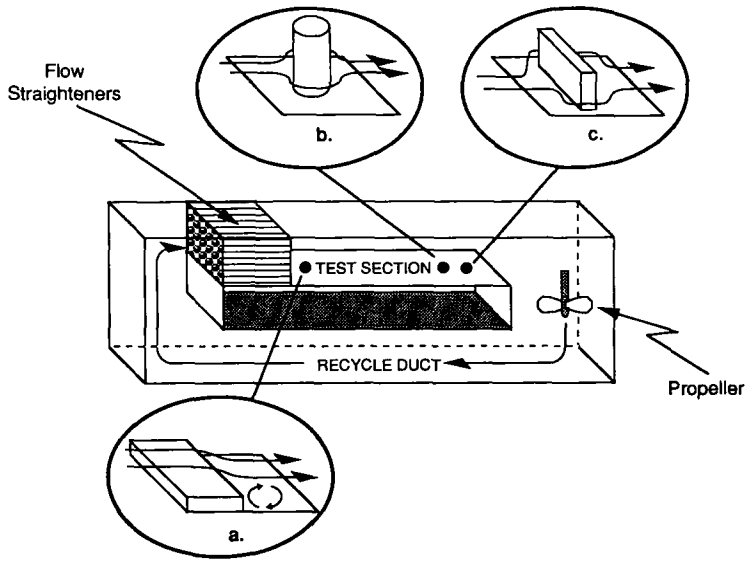


FIG. 1. Schematic diagram of the flow loop showing the placement of the: (a) backward-facing steps; (b) cylinder; (c) square plate on the floor of the channel.

In each mass uptake experiment, the edges of an 8 × 10 in. piece of sheet film were weighted down on the floor of the test section and after circulating a 50-fold diluted developer solution for 30 min, the film was removed for fixation. Uptake patterns were first recorded in the absence of any obstruction, both at the test section entrance and 51 cm downstream of the entrance. Then, experiments were carried out in the presence of four alternative flow obstructions—a 7.6 cm long × 0.95 cm high and a 7.6 cm long × 1.9 cm high backward-facing step overlapping the film at the test section entrance (Fig. 1(a)), a 3.2 cm diameter × 10.2 cm long cylinder resting vertically on the center of the film at 51 cm downstream of the entrance (Fig. 1(b)), and a 5.1 cm square × 0.8 cm thick flat plate in the same position as the cylinder (Fig. 1(c)).

## RESULTS AND DISCUSSION

*Resolution of the photographic method*

Resolution of the method was determined by comparing the optical densities measured during maximum (agitated) and minimum (non-agitated) mass transfer of developer to small film test strips. For a 5-fold dilution of stock solution (Fig. 2), the optical density in agitated developer rose rapidly and leveled off at 2.7 optical density units after 20 min. This asymptote represents the saturation level at which all silver grains are developed. Values of OD in non-agitated developer rose more gradually and appeared to approach the same saturation level, but after a much longer development time. Consequently, the difference in optical densities between agitated and non-agitated conditions is initially zero, is again zero at large times, and reaches a maximum value at some intermediate time. Experiments with 10- and 40-fold dilution of developer stock solution indicated that the OD value at saturation was the same at all dilutions, but the time required to reach saturation increased as the dilution ratio (i.e. 1/5, 1/10 and 1/40) decreased.

When the product of development time, $t$, and dilution ratio, $C$, was employed as a single independent variable, the OD data for agitated and non-agitated conditions could each be correlated by a single exponential equation (Fig. 3; lower panel). That is

$$OD = 0.13 + 2.65[1 - \exp(-1.09tC)] \quad (1)$$

for agitated developer and

$$OD = 0.13 + 2.65[1 - \exp(-0.313tC)] \quad (2)$$

for non-agitated developer. In equations (1) and (2), common optical density values for undeveloped film (OD = 0.13) and for saturated emulsion (OD = 2.78) are used since these are intrinsic characteristics of the film that should not depend on agitation conditions. The form of equation (1) suggests that the reduction of silver halide follows first-order kinetics with respect to the hydroquinone, and that the exponential constant of 1.09 is proportional to the reaction rate constant. The decline of this constant to a value of 0.313 when the developer is unagitated reflects an added limitation imposed by the diffusion resistance of hydroquinone through the aqueous phase.

The difference between OD values obtained in agitated and non-agitated developer corresponds to the overall resolution between very high and very low mass transfer rates (Fig. 3; upper panel). Employing equations (1) and (2), the overall resolution can be formulated in terms of the $tC$ product

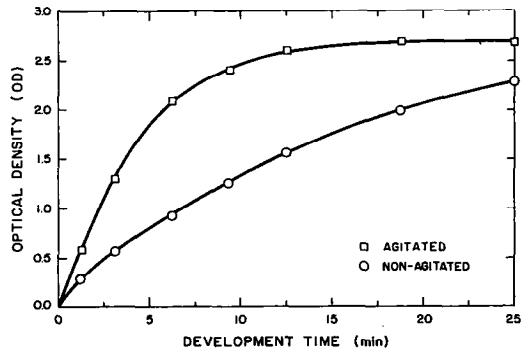


FIG. 2. Optical density of pre-exposed 100 ASA Plus-X film as a function of development time in a fivefold diluted D-76 solution. Solid curves were drawn by employing equations (1) and (2).

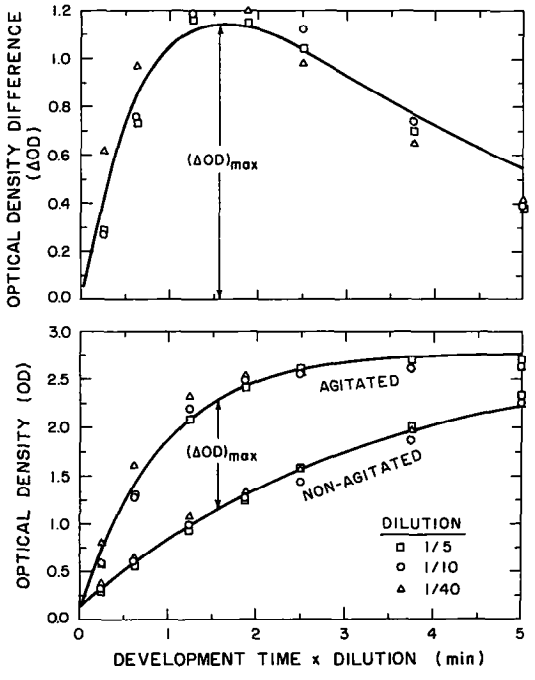


FIG. 3. Optical density as a function of the time–dilution product. Solid curves were drawn by employing equations (1)–(3). At a time–dilution product of 1.6, a maximum difference in optical density between agitated and non-agitated conditions, $(\Delta OD)_{max} = 1.1$, was observed.

$$\Delta OD = 2.65[\exp(-0.313tC) - \exp(-1.09tC)]. \quad (3)$$

Equation (3) predicts that overall resolution will have a maximum value of 1.1 optical density units when $tC$ is 1.6 min. At this optimal condition, equations (1) and (2) indicate that the agitated developer creates an OD approaching 83% of its saturation value while non-agitated developer leads to an OD which is only 42% of saturation. Therefore, the latitude of the film in recording variations in high mass transfer rates is much smaller than it is in recording low mass transfer rates. To reduce this non-linear effect, it is best to operate at a sub-optimal overall resolution with a time-dilution product less than 1.6.

In the open channel experiments, a development time of 30 min was chosen to avoid artifacts during the 1–2 min required to position and then remove the film from the floor of the test section. By selecting a developer dilution of 1/50, $tC$ had a value of 30(1/50) = 0.6 min. According to equations (1)–(3), the overall resolution would then be 0.82 optical density units, high mass transfer rates would lead to 58% saturation of the emulsion and low mass transfer rates would lead to 21% saturation.

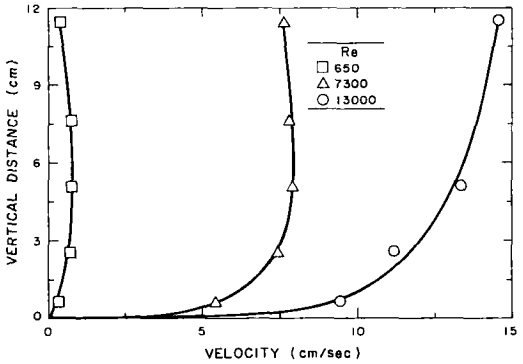


FIG. 5. Profiles of axial velocity for liquid flow at the midplane of the open channel. Measurements were made 51 cm downstream of the entrance of the channel. The midplane Reynolds number ($Re$) was computed as the ratio of an integrated velocity profile to the kinematic viscosity.

*Characterization of the open channel test section*

In the absence of flow obstructions, mass uptake patterns as well as dye-streakline movement were measured at the entrance of the open channel and at a point 51 cm downstream of the entrance. At the

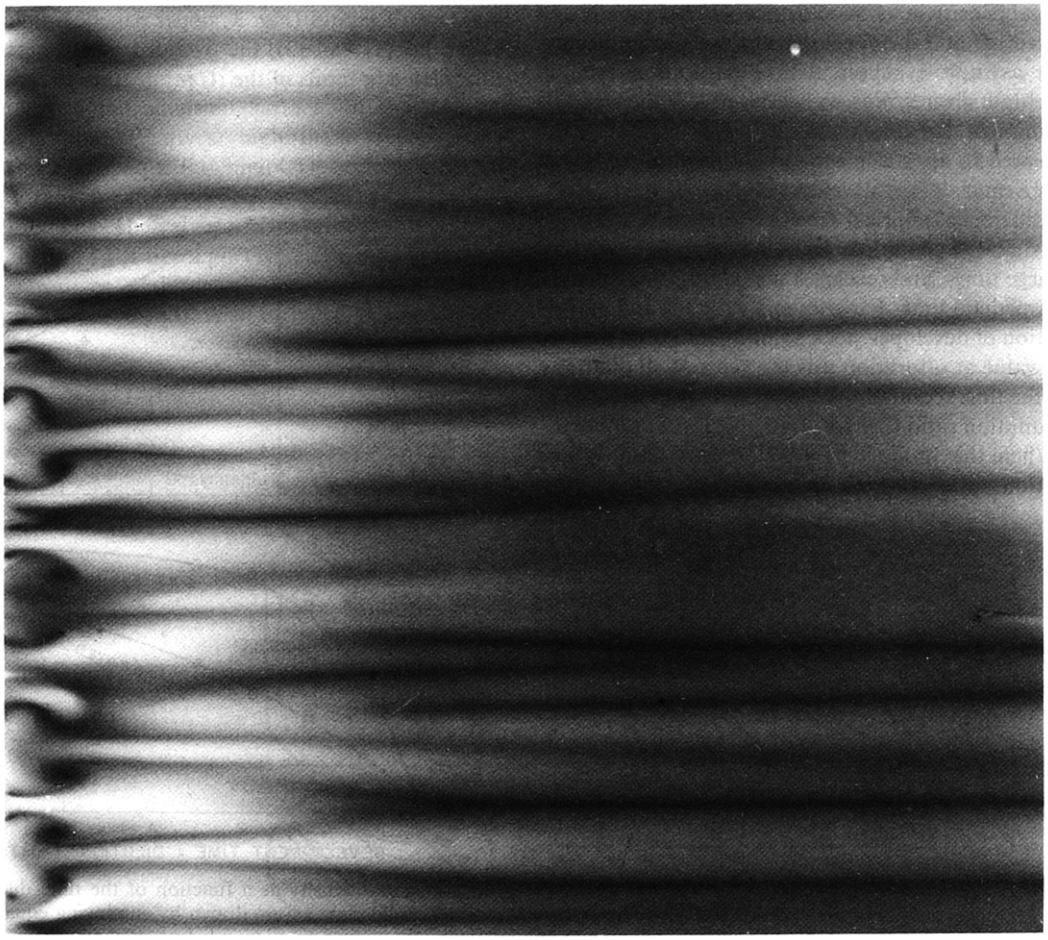

FIG. 4. Mass uptake pattern at the open channel entrance. The striations are due to liquid jetting through the soda straw flow straighteners. Flow is from left to right.

downstream position, mass uptake through the 8 × 10 in. area of the film was uniform with OD values of 0.70, 0.85, and 0.86 at the low, intermediate, and high propeller speed settings, respectively. On the other hand, mass uptake near the test section entrance was non-uniform, exhibiting a striated pattern (Fig. 4) due to jetting of liquid through the soda straw flow straighteners.

Midplane velocity profiles measured 51 cm downstream of the test section entrance are shown in Fig. 5. From left to right, these profiles correspond to the low, intermediate and high speed settings of the propeller motor. By numerically integrating these profiles with respect to vertical distance, midplane mean velocities of 0.51, 5.7 and 9.8 cm $s^{-1}$ conforming to the three propeller speeds were obtained. The corresponding midplane Reynolds numbers based on the 12.7 cm liquid depth are 650, 7300 and 13000. Due to the jetting of entering liquid, there was a rapid dispersion of dye tracer at the upstream end of the test section, and it was not possible to obtain reliable streakline measurements at this site. In lieu of these measurements, the discussion below ascribes the same Reynolds numbers to the upstream and downstream measurement sites.

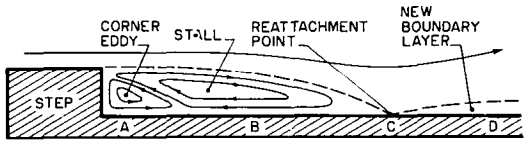


FIG. 6. General behavior of flow downstream of a backward-facing step.

*Mass uptake patterns created by flow obstructions*

The presence of flow obstructions on the floor of a channel can result in unexpected boundary layer behavior often producing adverse pressure gradients which lead to flow separation and vortex formation.

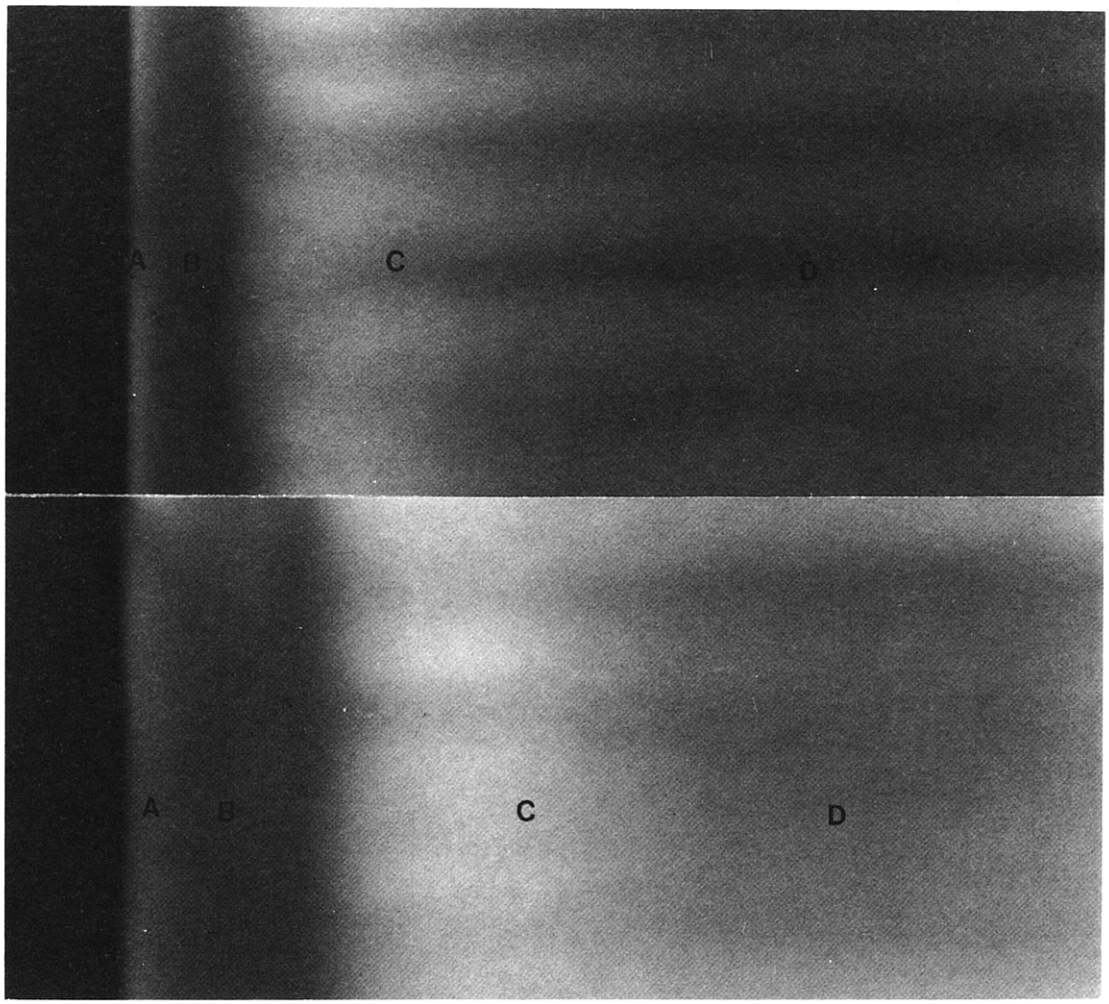


FIG. 7. Mass uptake pattern downstream of backward-facing steps at a Reynolds number of 13000. The steps were 0.95 cm (upper) and 1.9 cm (lower) in height and were positioned at the entrance of the open channel. The alphabetical labels in this figure are consistent with those labels in Fig. 6. Flow is from left to right.

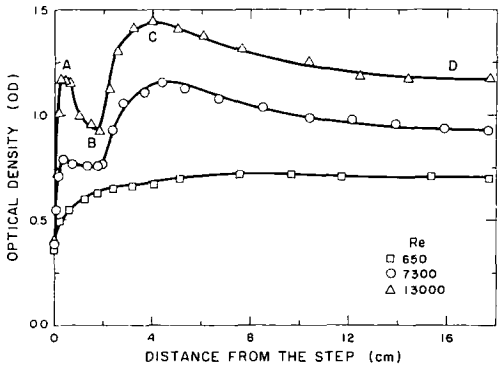


FIG. 8. Variation in optical density along the flow direction at the midline of the backward-facing step. This step was 0.95 cm in height and was positioned at the entrance of the open channel. The origin corresponds to the drop off of the step, and the alphabetical labels are consistent with the labels in Figs. 6 and 7.

Reattachment of the boundary layer may follow as soon as the adverse pressure gradient is weakened or replaced by a favorable one. In this work, three idealized geometries have been employed to demonstrate the nature of mass transfer patterns that can be produced by such complex flow phenomena.

1. *The backward-facing step.* The results of previous visualizations of flow over a backward-facing step [9, 10] are sketched in Fig. 6, positive prints of the mass uptake patterns for 0.95 and 1.9 cm high steps are shown in Fig. 7, and OD scans of negatives along the midline of the 0.95 high step at the three Reynolds numbers are compared in Fig. 8. In these figures, a corner eddy producing high mass transfer rates is located immediately downstream of the step (A), while an adjacent and much larger circulating stall is associated with a relative minimum in mass uptake (B). Downstream of the stall, the liquid reattaches to the bottom of the channel giving rise to a maximum mass transfer rate (C). Still further downstream, mass transfer decreases as a new boundary layer is formed (D).

Comparing the two mass transfer images in Fig. 7, it is clear that an increase in step height from 0.95 cm (upper panel) to 1.9 cm (lower panel) increases the diameters of the corner eddy and stall as well as the reattachment length of the boundary layer. Moreover, the OD scans in Fig. 8 demonstrate that increasing the

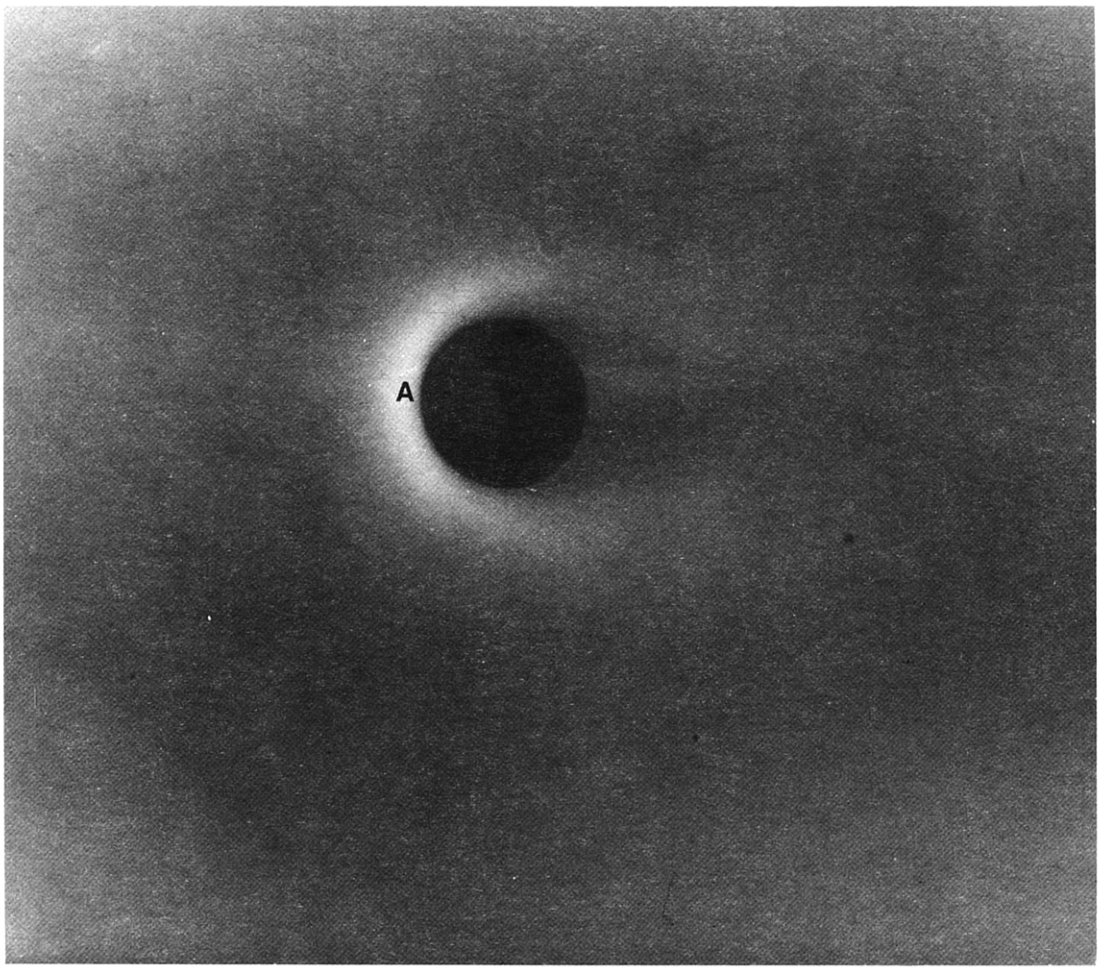


FIG. 9. Mass uptake pattern around the vertical cylinder at a Reynolds number of 650. The cylinder was positioned 51 cm downstream of the open channel entrance and flow was from left to right.

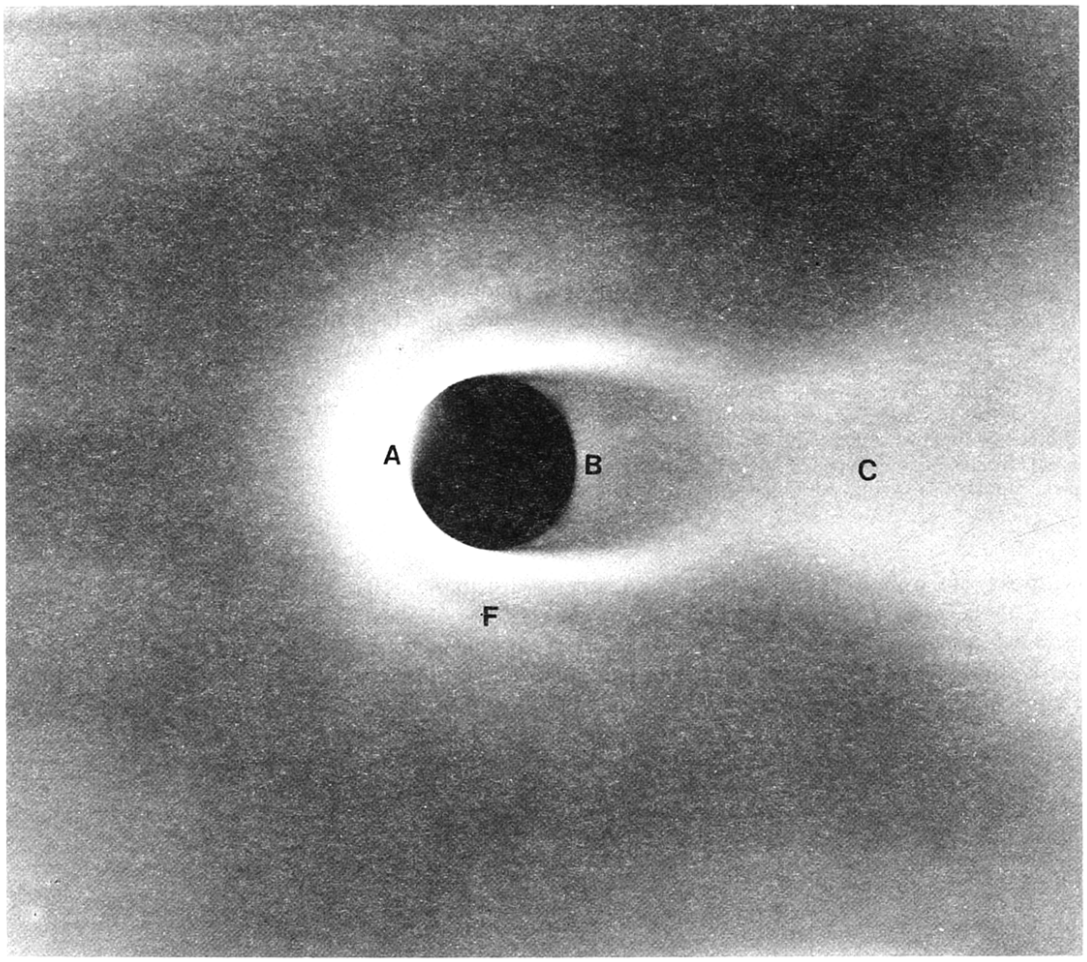


FIG. 10. Mass uptake pattern around the vertical cylinder at a Reynolds number of 13 000. The cylinder was positioned 51 cm downstream of the open channel entrance and flow was from left to right.

Reynolds number causes a significant and progressive augmentation of mass uptake by the corner eddy and at the reattachment point.

2. *The vertical cylinder.* The mass uptake pattern obtained for the vertical cylinder at a low Reynolds number is shown in Fig. 9. A horseshoe-shaped high mass transfer region is apparent at the circular junction between the cylinder and the floor of the channel. The horseshoe is whitest at the upstream side of the cylinder (A), possibly because a flow stagnation occurring at that point creates an intense corner eddy. The fading of the horseshoe around the circular perimeter is probably due to a weakening of this corner eddy. Although the horseshoe appears to detach from the rear surface of the cylinder, this reduction of mass transfer may actually be associated with boundary layer development on the floor of the channel rather than vortex formation in the bulk liquid above the floor. Nevertheless, it is interesting that this pattern is similar to the horseshoe vortex observed by Waka *et al.* [11] in their study of flow visualization around a freely-suspended circular cylinder.

At a high Reynolds number (Fig. 10), the downstream portion of the horseshoe merges with a white triangular wake-like structure (C) and also encloses a relatively high mass transfer region immediately behind the cylinder (B). Perhaps the most remarkable feature of this image is the presence of two light bands separated by a dark fringe (F) concentric with the horseshoe. Such a distinct mass uptake pattern would be a natural feature to use in verifying theoretically-based computer simulations.

From the OD scans along the midline of the cylinder (Fig. 11), it is clear that mass transfer is greatest at the frontal stagnation point (A) and, in the case of the high Reynolds number, mass uptake is nearly as great in downstream regions (B) and (C). The fringe (F) that appeared on the printed negatives was not sufficiently distinct along the cylinder midline to be resolved on the OD scan.

3. *Vertical square plate.* Mass uptake patterns for the vertical square plate shown in Figs. 12 and 13 are similar to those obtained for the vertical cylinder. A horseshoe-shaped high mass transfer region originates at the upstream contact line between the plate and the floor of the channel (A). At the high Reynolds number (Fig. 13), the horseshoe terminates in a wake (C), enclosing a high mass transfer region (B) immediately

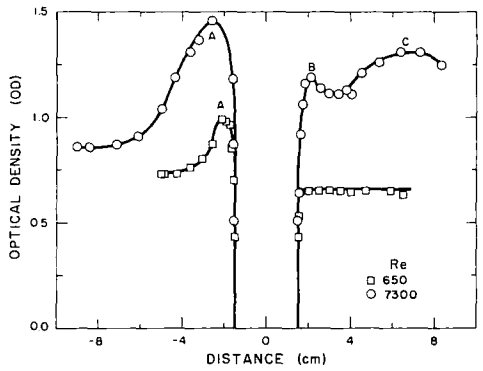


FIG. 11. Variation in optical density along the flow direction at the midline of the vertical cylinder. The cylinder was positioned 51 cm downstream of the open channel entrance. The 3.2 cm diameter cylinder is centered about the origin, and the alphabetical labels are consistent with the labels in Figs. 9 and 10.

downstream of the plate. At the low Reynolds number (Fig. 12), the downstream region enclosed by the horseshoe exhibits low and uniform mass uptake.

Dark fringes (F) appearing around the plate are more prominent than those observed around the cylinder. In fact, the increase from the low to the high Reynolds number generates an additional fringe. Even the OD scan in Fig. 14 clearly documents the presence of fringes.

## CONCLUDING REMARKS

The purpose of this study was to demonstrate that the flow of dilute developing solution over an exposed photographic film is a viable technique for the qualitative visualization of mass uptake patterns at solid surfaces. By comparing the optical density in films developed in highly-agitated and non-agitated solutions, we found that the overall resolution of the method between high and low mass transfer rates can be as high as 1.1 optical density units. Judging from the optical density patterns recorded in flows around a submerged cylinder and square plate, the resolution is adequate to discern subtle details of mass transfer distributions.

The application of the photographic method to problems in science and engineering are numerous. We are interested in characterizing mass uptake in mammalian cardiovascular and respiratory systems

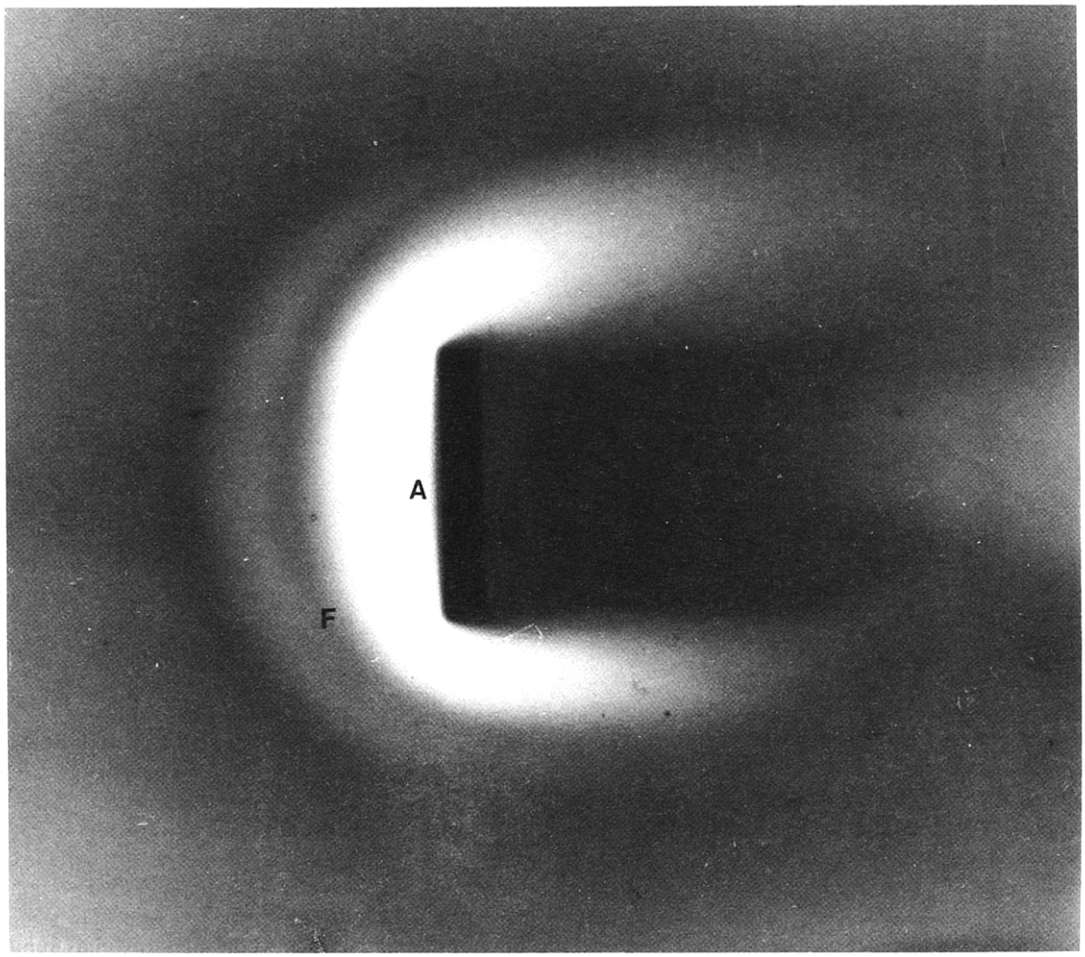


FIG. 12. Mass uptake pattern around the vertical square plate at a Reynolds number of 650. The plate was positioned 51 cm downstream of the open channel entrance and flow was from left to right.

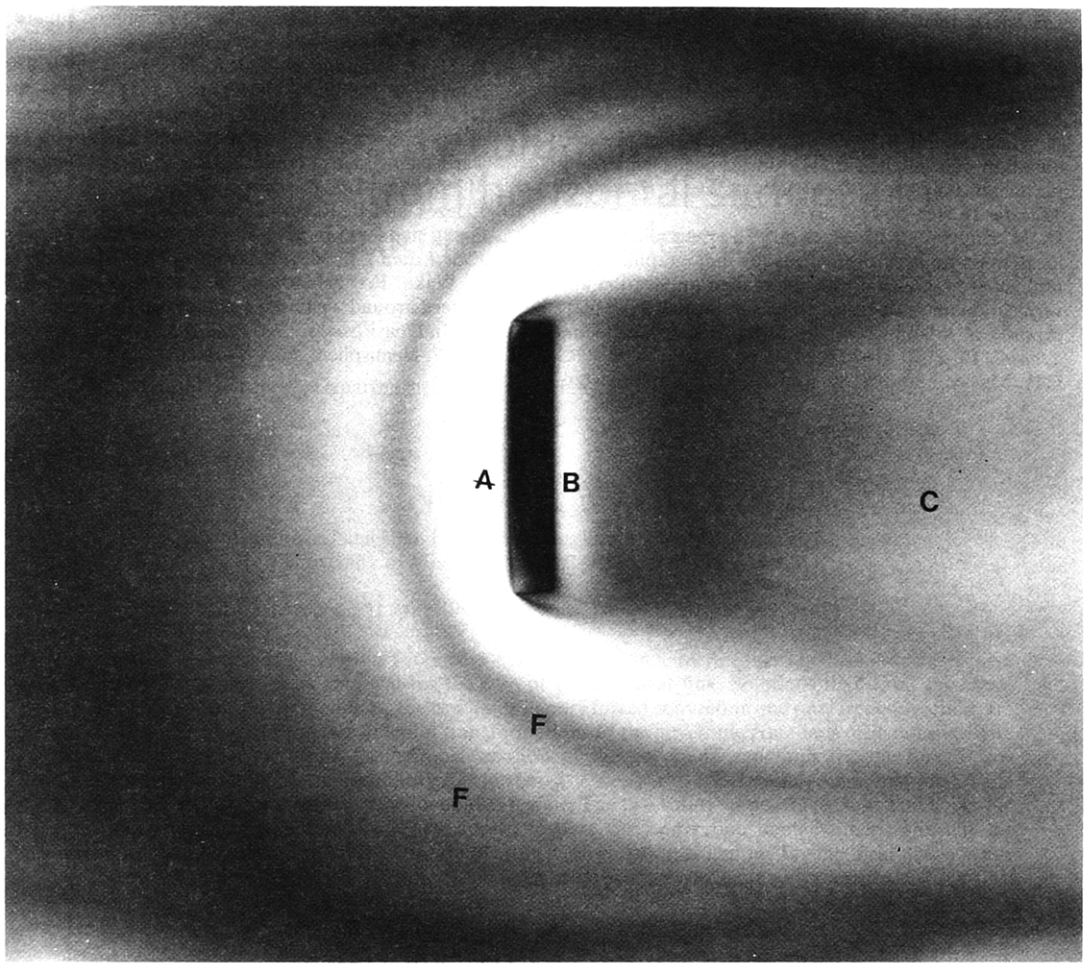


FIG. 13. Mass uptake pattern around the vertical square plate at a Reynolds number of 7300. The plate was positioned 51 cm downstream of the open channel entrance and flow was from left to right.

by using scaled-up physical models or casts of the relevant blood vessels and airways. Recently, there has been an increasing emphasis on solving problems in such complicated geometries by using numerical analysis rather than by making direct measurements.

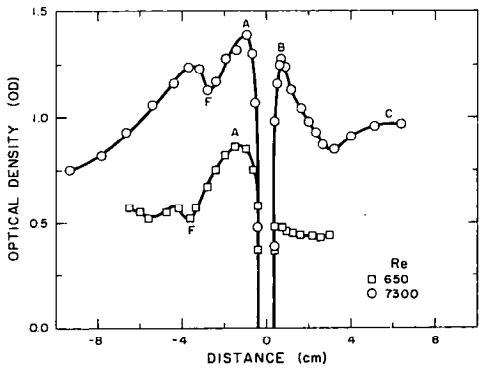


FIG. 14. Variation in optical density along the flow direction at the midline of the vertical square plate. The plate was positioned 51 cm downstream of the open channel entrance. The 0.8 cm thick plate is centered about the origin, and the alphabetical labels are consistent with the labels in Figs. 12 and 13.

However, the computer simulations always incorporate approximations that must themselves be verified by comparison to data. The photographic method can provide a convenient means to obtain such data.

*Acknowledgments*—The authors appreciate the invaluable assistance of Stephen Vogel and Carl Heine for advice on flow chamber design, Bobby Parker for construction of the flow chamber with important modifications, Donald Joyner for technical assistance, and Mel Andersen and Fred Miller for advice and encouragement. This work was made possible in part by a research grant from the Chemical Industry Institute of Toxicology to Penn State University.

## REFERENCES

1. T. Mizushina, The electrochemical method in transport phenomena. In *Advances in Heat Transfer* (Edited by T. F. Irvine, Jr. and J. P. Hartnett), Vol. 7, p. 87. Academic Press, New York (1971).
2. F. E. M. Saboya and E. M. Sparrow, Local and average transfer coefficient for one-row plate fin and tube heat exchanger configuration, *Trans. ASME* **96,** 265–272 (1974).
3. E. M. Sparrow and F. P. Kalejs, Local convective transfer coefficient in a channel downstream of a partially

constricted inlet, *Int. J. Heat Mass Transfer* **20,** 1241–1249 (1977).
4. N. Macleod, M. D. Cox and R. B. Todd, A profilometric technique for determining local mass-transfer rates, *Chem. Engng Sci.* **17,** 923–935 (1962).
5. N. Macleod and R. B. Todd, The experimental determination of wall–fluid mass transfer coefficients using plasticized polymer surface coatings, *Int. J. Heat Mass Transfer* **16,** 485–504 (1973).
6. D. N. Kapur and N. Macleod, The determination of local mass-transfer coefficients by holographic interferometry—I. General principles: their application and verification for mass-transfer measurement at a flat plate exposed to a laminar round air-jet, *Int. J. Heat Mass Transfer* **17,** 1151–1162 (1974).
7. J. H. Masliyah and T. T. Nguyen, Holographic determination of mass transfer due to impinging square jet, *Can. J. Chem. Engng* **54,** 299–304 (1976).
8. D. H. O. John and G. T. J. Field, *Photographic Chemistry*, p. 93. Reinhold, New York (1963).
9. D. E. Klein and S. J. Kline, Experimental investigation of subsonic turbulent flow over single and double backward facing steps, *Trans. ASME J. Basic Engng* **84D,** 317–325 (1962).
10. J. Jezek and R. Reznicek, Visualization of a backward facing step flow. In *Flow Visualization* (*Proc. Int. Symp. Flow Visual.*), p. 365. Hemisphere, New York (1977).
11. R. Waka, F. Yoshino and Y. Furuya, Visualized flow pattern around a circular cylinder with tangential blowing. In *Flow Visualization* (*Proc. Int. Symp. Flow Visual.*), p. 367. Hemisphere, New York (1977).